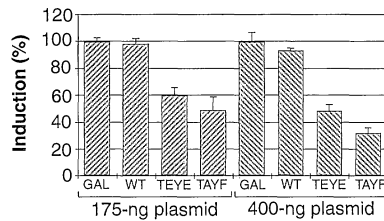


Fig. 4. Inhibition of IFN- β -stimulated transcription of an ISRE reporter plasmid in cells expressing dominant negative 42-kD MAPK. Primary human fibroblasts were transfected as described (17) with an ISRE derived from the IFN-stimulated responsive gene ISG15 linked 5' to a thymidine kinase minimal promoter-luciferase reporter (9). In addition to the reporter construct, plasmids containing complementary DNAs (cDNAs) corresponding to either wild-type MAPK (WT) or MAPK in which Thr¹⁸³ and Tyr¹⁸⁵ were replaced with either glutamic acid (TEYE) or alanine and phenylalanine (TAYF). These plasmids all contained a cytomegalovirus (CMV) promoter. To normalize for DNA in the transfection, a CMV-driven β -galactosidase cDNA (GAL) was included when the MAPK kinase plasmids were not present. The plasmids were used at either 175 ng/ml or 400 ng/ml in the transfection. Twenty hours after transfection, IFN- β (10^3 units/ml) was added to the cells for 6 hours before preparation of cell lysates and assay of luciferase activity. The amount of luciferase activity in the cells transfected with β -galactosidase and treated with IFN- β (which was consistently five- to sixfold that of untreated cells) was normalized to 100%. The reporter construct without the ISRE showed no increased luciferase activity in the presence of IFN- β . The standard deviations for these experiments are denoted by error bars.



quired to be phosphorylated for activity were replaced with either glutamic acid (TEYE) or alanine and phenylalanine (TAYF), rendering the proteins inactive (8). After transfection fibroblasts were incubated with or without IFN- β , the cells lysed, and luciferase activity assayed. Consistently, IFN- β stimulated a five- to sixfold increase in the luciferase activity in cells transfected with the ISRE containing the luciferase reporter. Co-transfection of wild-type MAPK with the reporter had little if any effect on IFN- β -stimulated luciferase activity, whereas the mutant MAPK constructs showed a dose-dependent inhibition of IFN- β -stimulated luciferase activity (Fig. 4). Thus, it appears that MAPK participates in the mechanism by which IFN- β stimulates early response genes that require activation of the STAT transcription factors.

Interleukin 6 induces serine phosphorylation of Stat3, which is required for binding of Stat3 homodimers to DNA (10). Although we have not observed a requirement of serine phosphorylation for ISRE binding of Stat1 α , treatment of U266 cells with IFN- β does stimulate serine phosphorylation of the protein (11). The serine-threonine kinase inhibitor H7 can selectively inhibit IFN- α activation of ISRE-dependent genes without affecting Stat1 and Stat2 binding to the ISRE (6, 12). These data, together with those of Zhang *et al.* (10), would suggest that IFN- α - or IFN- β -stimulated phosphorylation of both serine and tyrosine on Stat1 α is required for transactivation.

It remains to be established whether activation of MAPK is required to stimulate tyrosine phosphorylation of Stat1 and Stat2 by IFN- α and IFN- β . Our results indicate that one target of MAPK is a conserved phosphorylation site in the COOH terminus of Stat1 α , and possibly Stat3 and Stat4. Mapping of the interaction sites between the 42-kD MAPK and the STAT proteins will elucidate the role of MAPK in transcriptional activation of STAT-responsive genes.

Note added in proof: Recently, Wen *et al.* (18) reported that Ser⁷²⁷ in Stat1 is phosphorylated. Maximal transcriptional activation by IFN- γ requires that this serine be present in Stat1.

REFERENCES AND NOTES

1. A. C. Larner and D. S. Finbloom, *Biochim. Biophys. Acta* **1266**, 278 (1995).
2. J. N. Ihle *et al.*, *Trends Biochem.* **19**, 222 (1994).
3. M. David *et al.*, in preparation.

4. O. Colamonic *et al.*, *Mol. Cell. Biol.* **14**, 8133 (1994).
5. O. R. Colamonic *et al.*, *J. Biol. Chem.* **269**, 3518 (1994); S. N. Constantinescu *et al.*, *Proc. Natl. Acad. Sci. U.S.A.* **91**, 9602 (1994).
6. M. David *et al.*, unpublished data.
7. H.-C. Wang *et al.*, *Mol. Biol. Cell* **3**, 1329 (1992).
8. J.-H. Her *et al.*, *Biochem. J.* **296**, 25 (1993).
9. R. Pine *et al.*, *EMBO J.* **13**, 158 (1994).
10. X. Zhang *et al.*, *Science* **267**, 1990 (1995).
11. D. S. Finbloom and A. C. Larner, unpublished data.
12. N. C. Reich and L. M. Pfeffer, *Proc. Natl. Acad. Sci. U.S.A.* **87**, 8761 (1990).
13. Cells were diluted with ice-cold phosphate-buffered saline (PBS) and centrifuged at 1500g for 10 min at 4°C, washed with PBS, and resuspended in lysis buffer containing 20 mM Hepes (pH 7.4), 1 mM vanadate, 10 mM β -glycero-phosphate, 100 mM NaCl, 50 mM NaF, 1% Triton X-100, and 1 mM phenylmethylsulfonyl fluoride. The lysate was mixed, incubated on ice for 10 min, and centrifuged at 18,000g for 10 min at 4°C.
14. G. Uze, G. Lutfalla, I. Gresser, *Cell* **60**, 225 (1990).
15. K. Igarashi *et al.*, *J. Biol. Chem.* **269**, 14333 (1994).
16. The MBP was added to a buffer containing 20 μ M ATP, 20 mM Hepes (pH 7.4), 10 mM MgCl₂, 10 mM β -glycero-phosphate, 1 mM vanadate, 5 mM EGTA, and 1 μ Ci [γ -³²P]ATP.
17. E. F. Petricoin *et al.*, *Mol. Cell. Biol.* **12**, 4486 (1992).
18. Z. Wen *et al.*, *Cell* **82**, 241 (1995).
19. We thank D. Finbloom for his critical reading of the manuscript and O. Colamonic and J. Krolewski for the GST fusion protein constructs. M.J.W. acknowledges the support of grant GM47332, and R.P. was supported by the Arthritis Foundation and the Lucille P. Markey Charitable Trust.

20 June 1995; accepted 23 August 1995

Imaging Elementary Events of Calcium Release in Skeletal Muscle Cells

Alexander Tsugorka,* Eduardo Ríos,† Lothar A. Blatter

In skeletal muscle cells, calcium release to trigger contraction occurs at triads, specialized junctions where sarcoplasmic reticulum channels are opened by voltage sensors in the transverse tubule. Scanning confocal microscopy was used in cells under voltage clamp to measure the concentration of intracellular calcium, [Ca²⁺]_i, at individual triads and [Ca²⁺]_i gradients that were proportional to calcium release. In cells stimulated with small depolarizations, the [Ca²⁺]_i gradients broke down into elementary events, corresponding to single-channel currents of about 0.1 picoampere. Because these events were one-tenth to one-fifth the size of calcium sparks (elementary release events of cardiac muscle), skeletal muscle control mechanisms appear to be fundamentally different.

For muscles to contract, Ca²⁺ must be released from the sarcoplasmic reticulum (SR) rapidly and massively, through channels of the ryanodine receptor family (1) present also in neurons (2), endothelial (3), and other cells (4). In cardiac muscle, Ca²⁺ release is determined by the membrane potential-dependent entry of Ca²⁺ (5), whereas in skeletal muscle release is con-

trolled by membrane potential without Ca²⁺ entry (6, 7). In confocal images of Ca²⁺ from voltage-stimulated skeletal muscle fibers, we found elementary events of release apparently derived from the opening of single SR channels.

We adapted the single muscle fiber voltage clamp (8, 9) to work synchronously with a laser scanning confocal microscope. In a cell at rest (-90 mV) containing the Ca²⁺ indicator fluo 3, the banded pattern of fluorescence indicated greater access or binding of fluo 3 to specific regions of the sarcomere (Fig. 1A). Fluorescence along a line was scanned every 1.39 ms and successive scans plotted in a line scan image (Fig. 1B). The periodic dye distribution resulted

A. Tsugorka and E. Ríos, Department of Molecular Biophysics and Physiology, Rush University, Chicago, IL 60612, USA.

L. A. Blatter, Department of Physiology, Loyola University, Chicago, Maywood, IL 60153, USA.

*Permanent address: A. A. Bogomoletz Institute, Kiev, 24, 25260IGFP, Ukraine.

†To whom correspondence should be addressed.

in bands in the line scan image at early times, before pulses were applied. The application of small depolarizing pulses caused

the fluorescence to increase, revealing Ca^{2+} release. Early in the first pulse, when the release was large, the banded pattern re-

versed, which indicated that $[\text{Ca}^{2+}]_i$ increased more in the regions of lower concentration of dye, which therefore correspond to the triadic regions of the sarcomere (9).

The graphs in Fig. 1 summarize a macroscopic analysis of the image. First, fluo 3 fluorescence was averaged during each scan (Fig. 1C); average $[\text{Ca}^{2+}]_i(t)$, a function of time only, was calculated from the averaged fluorescence (Fig. 1D), and Ca^{2+} release flux was derived from $[\text{Ca}^{2+}]_i(t)$ (Fig. 1E) (10). Release during the second pulse was steady; a fast inactivating component was removed by the presence of the first pulse.

A wave form proportional to local Ca^{2+} release was obtained from single triad signals. As a function of space and time, $[\text{Ca}^{2+}]_i$ was derived from the line scan image, taking into account the known kinetics and diffusion properties of fluo 3 (11) (Fig. 2). This calculation essentially removed the banded pattern of the image before and after the pulses, which indicated that $[\text{Ca}^{2+}]_i$ was homogeneous at those times. In contrast, during the pulses pronounced gradients appeared in every sarcomere. During the second pulse (to -55 mV), the local increases in Ca^{2+} were much smaller and discrete.

On plots of $[\text{Ca}^{2+}]_i$ as a function of space and time (Fig. 3A), triads were localized as regions of higher $[\text{Ca}^{2+}]_i$ (9). Values for $[\text{Ca}^{2+}]_i(t)$ for one of the scanned triads were greater and had more noise than the averaged $[\text{Ca}^{2+}]_i(t)$ at the centers of both flanking sarcomeres (Fig. 3B). The difference of these (Fig. 3C), a measure of the local concentration gradient, should be roughly proportional to the flux of Ca^{2+} release from the individual triad. Indeed, the average of this triadic gradient over the 45 triads in the scan (Fig. 3D) is a blunted version of the macroscopic release (Fig. 1E).

Especially during the smaller pulse, individual triadic event records (Fig. 3C) show discrete events that might represent single-channel openings. The amplitude histogram of that record and similar records from 10 other triads was bimodal (Fig. 4).

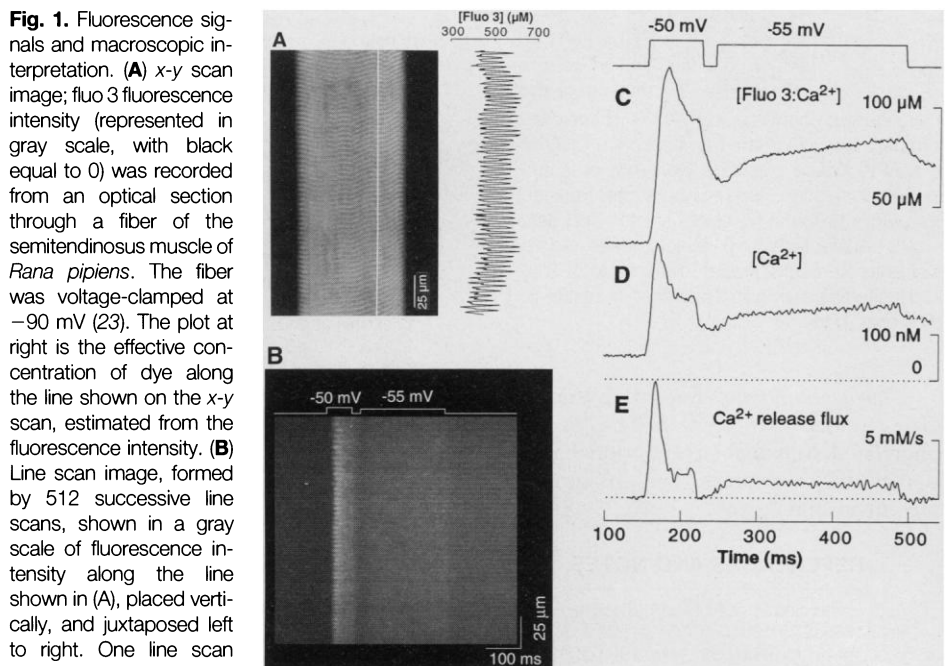


Fig. 1. Fluorescence signals and macroscopic interpretation. (A) x-y scan image; fluo 3 fluorescence intensity (represented in gray scale, with black equal to 0) was recorded from an optical section through a fiber of the semitendinosus muscle of *Rana pipiens*. The fiber was voltage-clamped at -90 mV (23). The plot at right is the effective concentration of dye along the line shown on the x-y scan, estimated from the fluorescence intensity. (B) Line scan image, formed by 512 successive line scans, shown in a gray scale of fluorescence intensity along the line shown in (A), placed vertically, and juxtaposed left to right. One line scan covered 512 spots placed $0.3 \mu\text{m}$ apart ($154 \mu\text{m}$). Because scans were taken at 1.39-ms intervals, the horizontal dimension, representing time, covers 712 ms. Two pulses, to -50 and -55 mV, were applied as shown at the top of the traces. (C) Spatial average of scanned intensity as a function of time. The average intensity was scaled to the average concentration of dye bound to Ca^{2+} , $[\text{dye}:\text{Ca}^{2+}]$, with

$$[\text{dye}:\text{Ca}^{2+}] = \text{dye}_T(F - F_{\min}) / (F_{\max} - F_{\min})$$

where dye_T is the total dye concentration and F_{\min} and F_{\max} are the minima and maxima of fluorescence, corresponding to Ca^{2+} -free and Ca^{2+} -saturated fluo 3 (24). (D) Spatial average of free Ca^{2+} concentration, derived from the average fluorescence as

$$[(k_{\text{on}}^{-1}dF/dt + K_d(F - F_{\min})) / (F_{\max} - F)]$$

where k_{on} is the Ca^{2+} :dye association rate constant and K_d the dissociation constant; k_{on} and K_d were determined inside the fiber in simultaneous experiments with fluo 3 and a fast absorption dye (25). (E) Ca^{2+} release flux, determined from the Ca^{2+} record (D) (10, 15).

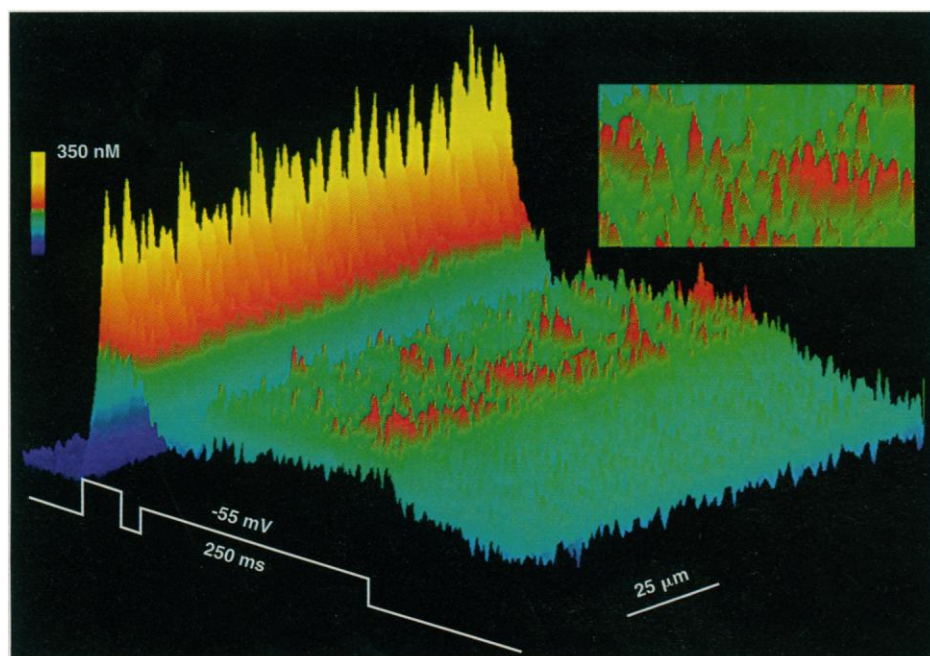
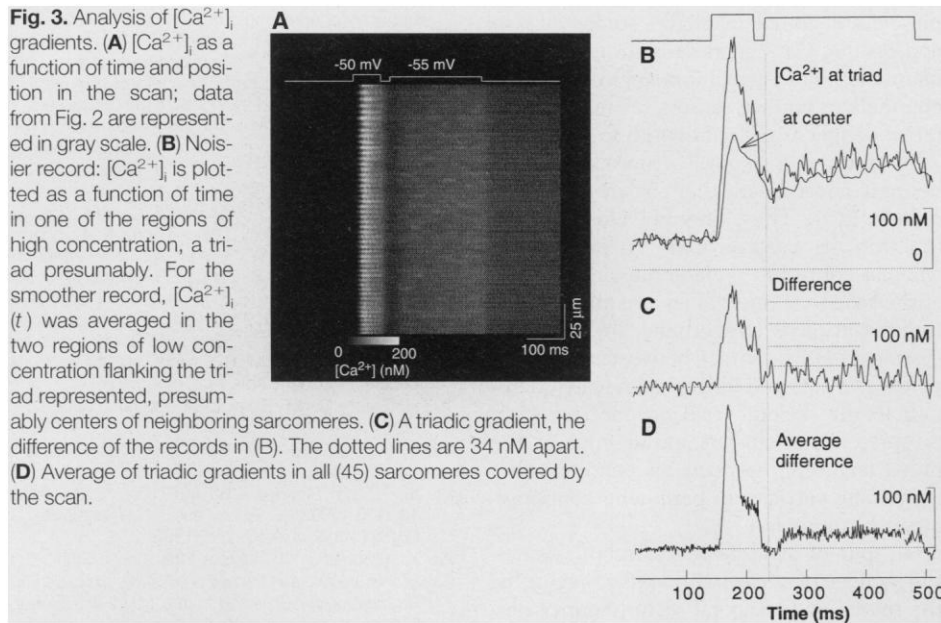


Fig. 2. Distribution of Ca^{2+} . Intracellular Ca^{2+} concentration is represented as a function of time and position in the scan, derived from a line scan image (Fig. 1B). The inset expands the plot in a region where discrete events were visible during the second pulse. $[\text{Ca}^{2+}]_i$ was derived by solving numerically the partial differential equation that describes the evolution of $[\text{dye}:\text{Ca}^{2+}]$, namely

$$\partial[\text{dye}:\text{Ca}^{2+}]/\partial t = [\text{dye}][\text{Ca}^{2+}]k_{\text{on}}$$

$$- [\text{dye}:\text{Ca}^{2+}]k_{\text{off}} + D_{\text{dyeCa}}\Delta[\text{dye}:\text{Ca}^{2+}]$$

where D_{dyeCa} is the diffusion coefficient of the complex ($0.2 \times 10^{-6} \text{ cm}^2 \text{ s}^{-1}$) (11) and Δ is the Laplacian (26).



The curve is the sum of a baseline Gaussian curve centered near 0 and a second Gaussian curve centered at 28 nM above the baseline. This modal value of the triadic

gradient corresponds to a preferred magnitude of release flux from these triads (12).

If this level corresponds to flux through a single channel or an irreducible group of channels, it must satisfy criteria of voltage independence (because the SR membrane is not polarized) and superposition (increase

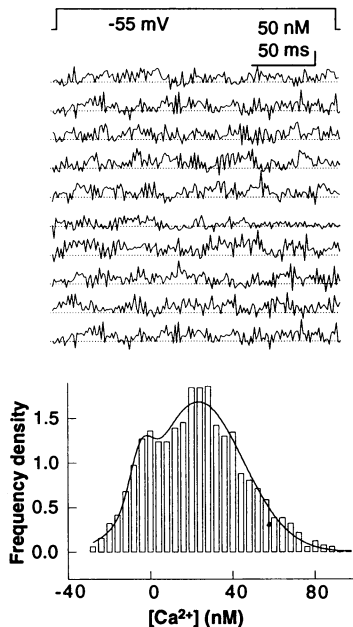


Fig. 4. Two predominant amplitudes in the triadic gradient. Top: triadic gradients from Fig. 3A for 10 individual triads during the depolarization to -55 mV. Bottom: amplitude histogram of all records during the pulse to -55 mV. Frequency density is the percent frequency of events per unit increment in Ca^{2+} concentration. The continuous line is an unrestricted fit of the histogram as the sum of two Gaussian curves; μ , the mean, and σ , the standard deviation, were -4.7 and 5.5 nM for the baseline and 23.3 and 21 nM for the second component, respectively. The baseline before the pulses was fitted with a Gaussian curve at -2 nM, with $\sigma = 6.1$ nM.

in activity should result from the increase in the number of events). The increase in $[\text{Ca}^{2+}]_i$ in one fiber depolarized to -55 mV was two times greater than that at -58 mV (Fig. 5, A and B). The corresponding amplitude histograms (Fig. 5, C and D) reflect the greater activation caused by the larger pulse, but the mode is in both cases at 21 nM, which demonstrates that the average size of the discrete events did not change with voltage. The broader distribution at the higher voltage seems to arise by superposition of discrete events, as the histogram at -55 mV was well fitted by the sum of three Gaussian curves (centered at 0, 21, and 50 nM). In five fibers, the "first open" level (the first nonzero mode in the histogram of triadic gradient amplitudes) ranged from 21 to 33 nM. In three of these fibers, multi-Gaussian distributions could be fitted at different voltages, and in all cases the first open level was independent of voltage. Thus, the increase of release with voltage appeared to occur by recruitment, rather than by an increase in the magnitude of the discrete event.

The early burst of activity observed in every pulse at -55 mV and at greater depolarization seemed in many cases to result from the superposition of discrete events (Fig. 3C). Thus, the early inactivating por-

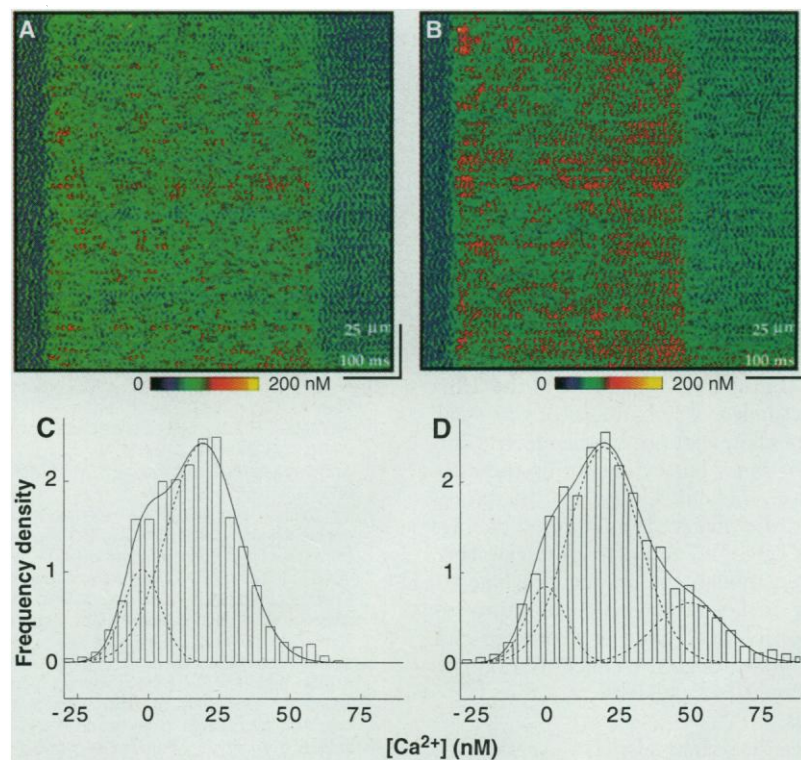


Fig. 5. $[\text{Ca}^{2+}]_i$ at two voltages. Left, events at -58 mV; right, at -55 mV. (A and B) $[\text{Ca}^{2+}]_i$ derived from line scan images. Because the activation of release is so low, bulk $[\text{Ca}^{2+}]_i$ hardly increases, and the release events become visible without subtraction. (C and D) Amplitude histograms of triad gradient records from (A) and (B), respectively. Frequency density is as in Fig. 4. Continuous curves are sums of the Gaussian curves shown in dashed lines. Parameters for (C) are as follows: $\mu = -2$ and 19 nM; $\sigma = 7$ and 13 nM. For (D) they are $\mu = 0, 21,$ and 50 nM and $\sigma = 7, 12,$ and 12 nM.

tion of release may be an accumulation of events of the same amplitude as those constituting the maintained phase of release. This would not support the idea that the two phases of release correspond to two different types of channels (13), unless both had the same open channel current.

The elementary events are probably caused by openings of single release channels. The confocal spot that scanned the image was 300 nm in diameter, close to the theoretical resolution of the microscope. It should intersect in every triad about 15 tetrads of voltage sensors (14), which are some 40 nm apart on both sides of a transverse (T) tubule. About 40 SR Ca^{2+} release channels are located in that space. Therefore, single-channel activity should become noticeable at levels of activation below 2 to 3% of the maximum, approximately the activation elicited by the pulses to -55 mV (15).

We estimated the release flux underlying an elementary event by comparing the macroscopic record (Fig. 1E) and the microscopic average (Fig. 3D). The Ca^{2+} release flux from the whole scanned region was about 1 mM/s during the small pulse (Fig. 1E). This corresponded to a local $[\text{Ca}^{2+}]_i$ gradient of about 30 nM on average (Fig. 3D). The average number of event-producing units that are open or active per triad is $N_j p_o$, where N_j is the number of units in a triad and p_o their average open probability. Because the first open triadic gradient level was also close to 30 nM (Fig. 3), the average number of open units or channels was nearly one per triad during the pulse. Hence, 1 mM/s is the (macroscopic) Ca^{2+} release flux when one unit is open in every triad. This corresponds to a flux per unit of approximately 10^{-18} mol/s, or 0.1 pA (16). This current is much less than available estimates for the current through a single cardiac release channel (17). Therefore, the event-producing unit is unlikely to be more than one channel.

We have thus quantified the flux through single Ca^{2+} channels (or very small groups of channels) not by the electric current they carry, but by measuring the associated ion gradient. Crucial to this procedure was the observed similarity of average gradient (Fig. 3D) and average release (Fig. 1E). Even though the uniquely regular periodicity of skeletal muscle made this averaging possible, the basic procedure of estimating flux through the concentration gradient should be applicable to other Ca^{2+} channels.

For cardiac channels, Ca^{2+} sparks (18) of rat and ferret heart myocytes (measured with the same microscope and dye) were 5- to 10-fold larger than the elementary events shown here (19) and required no stimulation (18). Because currents through single-release channels from cardiac and skeletal

muscle are similar in bilayer studies (1), it appears that Ca^{2+} sparks arise from multiple channels. The stoichiometry of release channels to voltage sensors (as revealed by ratios of specific dihydropyridine to ryanodine binding) is about 10 times greater in rat and ferret heart than in frog skeletal muscle (20). Thus, channel clusters may function in cardiac Ca^{2+} release (21), whereas control in skeletal muscle is apparently based on individual channels. This interpretation is strengthened by the suggestion (14) of contact between tetrads of voltage sensors and individual release channels in the skeletal triad, in contrast with the presence of clusters and absence of detailed matching between SR channels and membrane particles in peripheral couplings of cardiac muscle (22).

In spite of the differences, in both tissues the increase of release with voltage occurs by the spatial and temporal recruitment of observable unitary events (18). Studies of this recruitment should help elucidate the basic aspects of function, including the connection between the inactivating and steady components of release flux and the manner in which the gating of release is affected by locally elevated $[\text{Ca}^{2+}]_i$.

REFERENCES AND NOTES

- G. Meissner, *Annu. Rev. Physiol.* **76**, 485 (1994).
- R. H. Ashley, *J. Membr. Biol.* **111**, 179 (1989); G. Giannini, E. Clementi, R. Ceci, G. Marziali, V. Sorrentino, *Science* **257**, 91 (1992); Y. Hakamata, J. Nakai, H. Takeshima, K. Imoto, *FEBS Lett.* **312**, 229 (1992).
- R. E. Lesh, A. R. Marks, A. V. Somlyo, S. Fleischer, A. P. Somlyo, *Circ. Res.* **72**, 481 (1993).
- Y. Ogawa, *Crit. Rev. Biochem. Mol. Biol.* **29**, 229 (1994); V. Sorrentino and P. Volpe, *Trends Pharmacol. Sci.* **14**, 98 (1993).
- A. Fabiato, *Am. J. Physiol.* **245**, C1 (1983); M. Näbauer, G. Callewaert, L. Cleemann, M. Morad, *Science* **244**, 800 (1989).
- M. F. Schneider, *Annu. Rev. Physiol.* **56**, 463 (1994).
- E. Ríos and G. Pizarro, *Physiol. Rev.* **71**, 849 (1991).
- L. Kovacs, E. Ríos, M. F. Schneider, *Nature* **279**, 391 (1979); G. Brum, E. Ríos, E. Stefani, *J. Physiol. (London)* **398**, 441 (1988).
- A. L. Escobar, J. R. Monck, J. M. Fernández, J. L. Vergara, *Nature* **367**, 739 (1994).
- W. Melzer, E. Ríos, M. F. Schneider, *Biophys. J.* **45**, 637 (1984); *ibid.* **51**, 849 (1987).
- A. B. Harkins, N. Kurebayashi, S. M. Baylor, *ibid.* **65**, 865 (1993).
- Single-channel openings are expected to produce a constant gradient after a brief lag (21), especially in the presence of high concentrations of EGTA, which provides a dominant sink always far from equilibrium (7). Channels from triads inside the scanned spot should give signals of about the same size. Channels in the same Z line, but outside the spot, will give signals of smaller size and obscure and shift the main open level. A main open level was still discerned, perhaps because the probability of simultaneously activating neighboring channels in the same Z line was very small at the voltages where the level was discernible.
- E. Ríos and G. Pizarro, *News Physiol. Sci.* **3**, 223 (1988).
- B. A. Block, T. Imagawa, K. P. Campbell, C. Franzini-Armstrong, *J. Cell Biol.* **107**, 2587 (1988).
- A. González and E. Ríos, *J. Gen. Physiol.* **102**, 272 (1993).
- If one fully open channel per triad increases the myoplasmic Ca^{2+} concentration at 1 mM/s, the individual open channel must deliver Ca^{2+} at a rate of 1 mM/s multiplied by the myoplasmic volume associated with one triad. There is one triad for every sarcomere (length, 3.3 μm). The confocal spot was 0.3 μm in diameter, and the depth of the optical section was nearly 1 μm . Thus, the associated volume was about 1 μm^3 and the flux 10^{-18} mol/s per channel.
- A. Tinker, A. R. G. Lindsay, A. J. Williams, *J. Gen. Physiol.* **100**, 495 (1992).
- H. Cheng, W. J. Lederer, M. B. Cannell, *Science* **262**, 740 (1993); J. R. López-López, P. S. Shacklock, C. W. Balke, W. G. Wier, *J. Physiol. (London)* **480**, 21 (1994); M. B. Cannell, H. Cheng, W. J. Lederer, *Biophys. J.* **67**, 1942 (1994); P. Lipp and E. Niggli, *Circ. Res.* **74**, 979 (1994); J. R. López-López, P. S. Shacklock, C. W. Balke, W. G. Wier, *Science* **268**, 1042 (1995); M. B. Cannell, H. Cheng, W. J. Lederer, *ibid.*, p. 1045.
- H. Satoh, D. M. Bers, L. A. Blatter, unpublished results.
- D. M. Bers and V. M. Stiffel, *Am. J. Physiol.* **264**, C1587 (1993).
- M. D. Stern, *Biophys. J.* **63**, 497 (1992); *Cell Calcium* **13**, 183 (1992); E. Neher and G. J. Augustine, *J. Physiol. (London)* **450**, 273 (1992).
- X. H. Sun *et al.*, *J. Cell Biol.* **129**, 979 (1995).
- Procedures were as follows: A cut skeletal muscle fiber segment, singly dissected from a frog (*Rana pipiens*) killed under deep phenobarbital anesthesia, was voltage-clamped on the cover slip bottom of a two-Vaseline-gap chamber (9) that was mounted on the stage of a laser scanning confocal microscope (LSM 410; Zeiss, Oberkochen, Germany). The external solution had CH_2SO_2 (130 mM), tetraethylammonium (122.5 mM), Ca^{2+} (10 mM), plus blocking quantities of tetrodotoxin, 3,4-diaminopyridine, and 9-anthracene carboxylic acid. The internal solution had glutamate (100 mM), Cs^+ (125 mM), Mg^{2+} (5.5 mM) adenosine triphosphate (5 mM), fluo 3 (0.5 nM), EGTA (10 mM), glucose (5 mM), and phosphocreatine (5 mM), with Ca^{2+} added for a $[\text{Ca}^{2+}]_i$ of 50 nM. Both had 10 mM HEPES, were titrated at pH 7, and then adjusted to 270 and 260 mosmol/kg, respectively. Experiments were done at 13°C. Contractile movement was prevented by stretching (3.4 to 3.8 μm per sarcomere) and high concentrations of EGTA. A master computer (PC clone) generated pulses and acquired electrophysiological data as previously described (15) and synchronized the scanning microscope. Excitation light, from the 488-nm line of an argon laser, was delivered through a 40 \times , 1.0 numerical aperture objective. Fluorescence intensity above 515 nm was acquired. x-y and line scan images were acquired with pinholes at the setting prescribed to obtain a confocal optical slice between 0.8 and 1.0 μm deep.
- $F_{\min}(x)$ and its average F_{\min} were derived from the equilibrium relation

$$[\text{Ca}^{2+}](x) = K_d[F(x) - F_{\min}(x)]/[F_{\max}(x) - F(x)]$$
 applied to the resting situation, so that

$$F_{\min}(x) = F_o(x)(K_d + [\text{Ca}^{2+}]_o)/(K_d + R[\text{Ca}^{2+}]_o)$$
 where $F_o(x)$ is the resting fluorescence, $[\text{Ca}^{2+}]_o$ is the resting $[\text{Ca}^{2+}]$ (assumed equal to 0.05 μM), $R = F_{\max}/F_{\min} = 64.0$ (measured in a cuvette), and K_d is the dissociation constant.
- N. Shirokova, J. García, G. Pizarro, E. Ríos, *J. Gen. Physiol.*, in press.
- The Laplacian of $[\text{dye}:\text{Ca}^{2+}]$ was approximated by $3(\partial^2[\text{dye}:\text{Ca}^{2+}]/\partial x^2)$. The expression assumed the second derivative in the two directions of space perpendicular to the scan to be equal to the measured second derivative along the x direction—hence the factor of 3. This factor could be set to between 2.5 and 3 with no visible changes.
- We thank D. Chen for generous assistance in data processing, F. Cohen and N. Shirokova for helpful suggestions on the manuscript, and D. Bers for support and encouragement. Supported by grants from NIH (USA), the American Heart Association, and Schwappe Foundation Chicago (L.A.B.) and NIH, the American Heart Association, and the Muscular Dystrophy Association of America (E.R.).

10 May 1995; accepted 30 August 1995